

# Use of Computational Fluid Dynamics to Reduce Particulate Emissions from Wood-Fired Hydronic Furnace

Paul E. Glanville, Michael J. Kirby

Faculty: Dr. John C. Kramlich

Master's Level

University of Washington, Department of Mechanical Engineering, Box 352600, Seattle, WA 98195-2600

## ABSTRACT

Wood is a valuable but often overlooked energy resource, and two major challenges facing its use are obtaining efficient heat extraction and minimizing particulate emissions. This study examines the source of particulate emissions from an outdoor residential natural-draft cord wood-fired hydronic furnace. We use a Computational Fluid Dynamic (CFD) model to identify potential emission reductions and suggest furnace modifications. Wood pyrolysis gas entering the gas-phase combustion field is modeled as both a surrogate molecule and mixture of five constituents: CH<sub>4</sub>, CO, CO<sub>2</sub>, H<sub>2</sub>O, and H<sub>2</sub>, and various approaches for modeling the pyrolysis rate were explored. Combustion is modeled with both equilibrium mixture fraction and finite-rate eddy-dissipation approaches for 2D and 3D steady state solutions. Air starvation during the initial combustion phase and inadequate mixing were identified to be the primary sources of particulate emissions. Following recommendations of the model, the stoichiometry was adjusted, the secondary air pathways were introduced (i.e. overfire air), a compact heat exchanger was designed to provide longer residence times, and enhanced mixing was implemented for post-flame gases. These modifications lead to a reduction in test-averaged particulate matter emissions of 29% with EPA Method 28 testing. The exhaust path geometry modifications to aid mixing and secondary air placement reduced test-averaged stack temperatures, an indication of increased thermal efficiency, and increased turbulent mixing. With respect to the model, the use of mixture fraction modeling techniques consistently overestimates internal temperatures, and thus the superficial velocities. Coupled with the increasing computational power of personal computers, CFD proved to be a useful tool in the identification of emission problems and design of their solutions.

## INTRODUCTION

In light of the increasing cost of fossil fuels, the consequences of their use, impending U.S. Climate Change regulations, and a consumer demand for domestically available “Green” sources of energy, our attention has returned to wood as a viable source of heat and power. Wood is already a significant source of heat for domestic use, used at 18% of single-family homes in the U.S. for an energy output totaling 0.36 Quadrillion Btu/yr<sup>1</sup> (105.5 TWh thermal/yr). Wood is typically burned in batch mode in a bed configuration, and these systems can be significant sources of particulate matter (PM) emissions. The major challenges have been to design systems that (1) provide high heat recovery efficiency, (2) do so without excessive PM emissions, (3) are easy for the owner to use, and (4) do not involve excessive capital cost for hardware.

The Outdoor Wood-fired Hydronic Heater (OWHH) is an alternative to more simple systems like wood stoves and fireplaces. It makes use of a circulating water system to efficiently extract heat from the flue gas and flexibly deliver the heat to a variety of locations. In the OWHH, the wood is burned as a batch process in a fixed-bed combustor, where the fuel load is replenished roughly every 8-12 hours. While batch systems are easy for the consumer to use, this presents a challenge to the engineer to design a system optimized for different stages of wood combustion. Wood is generally considered to burn in four distinct, but overlapping stages<sup>2</sup>:

- 1) Heating and drying – Moisture is driven off and the solid fuel is brought to the temperature needed to begin pyrolysis
- 2) Solid-phase pyrolysis – Thermal degradation of organic material begins, releasing high molecular weight volatile species
- 3) Gas-phase pyrolysis and oxidation – Further degradation of volatile species occurs and radical species are generated, which combine with oxygen at the flame front to form product species
- 4) Char oxidation – Once volatiles are driven off, direct combustion of black carbon occurs

Broadly speaking, PM formation is either the result of incomplete combustion of primary particles produced by wood pyrolysis (producing Organic Carbon, or OC), or the nucleation of inorganic species coupled with their failure to burn out later (producing Black Carbon (soot), or BC).<sup>3</sup> It is worth distinguishing between the Organic Carbon (OC) and Black Carbon (BC) PM, or soot, as the composition of Red Oak PM emissions are 90% OC and 4% BC<sup>3</sup>. Because of this, the OC portion is the focus of this study and is to be referred to exclusively as ‘PM formation’. The OC portion is generated primarily during the gas-phase pyrolysis and oxidation stage, however the dynamics of this stage are directly affected by the previous two stages. A pathway mechanism suggests that tars and heavy organic species released during the second stage escape unburned due to flame quenching or excessive strain, also emitted are oxygenated polycyclic aromatic hydrocarbons (PAHs) and carbon monoxide (CO)<sup>4</sup>. Therefore, improving combustion efficiency acts to reduce PM emissions.

To model the gas-phase reactions and thermal transport, a Computational Fluid Dynamic (CFD) software package is employed to simulate the turbulent flow field specific to the OWHH geometry and operating conditions. The flame may be thought of as a buoyancy-dominated non-premixed reacting plume, for which the flow field is characterized by marked instabilities and a tight coupling between the smallest dissipative and the largest rotational scales of motion. In addition to the gas phase reactions, several studies also included the use of empirically derived solid phase pyrolysis sub-models, including Galgano et al. (2006)<sup>5</sup>, Huttenen et. al. (2006)<sup>6</sup>, and Bai et al. (2002)<sup>7</sup> with mixed successes. This study focuses on the gas-phase only.

The model is benchmarked against Environmental Protection Agency (EPA) Test Method 28<sup>8</sup> data from a commercially available OWHH, the using both a White Oak test crib configuration and Douglas Fir cordwood (unsplit log segments). Upon selection of appropriate modeling configurations and parameters, the sources PM formation are identified. This information is used to suggest modifications to the furnace and its operating conditions to close the pathways that allow PM to escape. These modifications are then validated via further experimentation. Thus, the goal of the study is to use the model and the experiment in conjunction to identify means to reduce PM emissions.

## BENCHMARK MODELING

In determining the how to model the OWHH, thus forward “furnace”, three separate facets must be addressed: how to chemically characterize the wood during the various phases of the burn, how to assess the heat transfer within the unit, and how to accurately capture the physics of the turbulent flow field and its effect on the previous two facets. While PM formation and oxidation are of interest, it is not to be modeled directly. A computational soot model grounded in physics that is not semi-empirical has not yet been developed<sup>9</sup> and the OC portion of PM formation is poorly understood<sup>2</sup>. As discussed in reference to PM formation, overall combustion efficiency is directly tied to PM formation and oxidation and may be assessed in simulation; therefore it is selected as a metric for PM emission reductions.

Figure 1: Furnace Interior and Thermocouple Locations

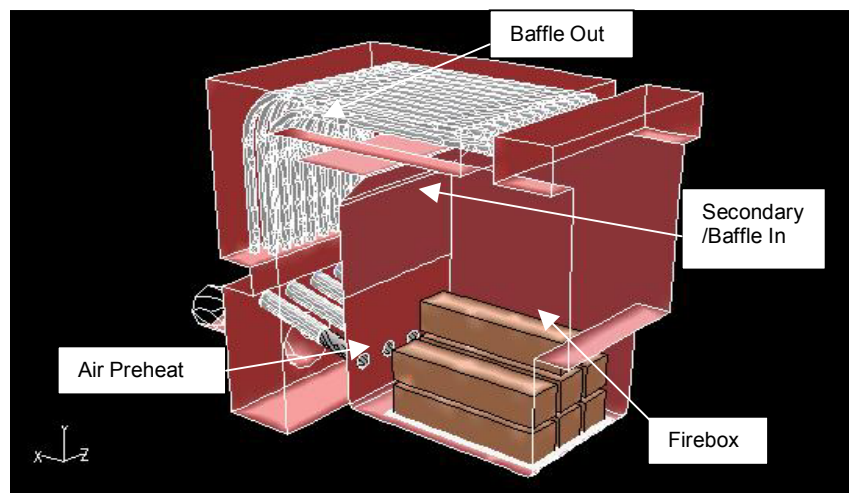


Figure 1 shows the interior of the furnace with a “cribwood” test crib, and this can be used as a guide to the operation of the unit and the setup for the CFD domain. The labeled zones represent internal thermocouple locations used during testing. During operation, preheated air enters as a natural draft through four inlet tubes into the preheated firebox composed of refractory brick. Radiation from the refractory back to the wood causes pyrolysis and the release of fuel gases. In turn, a buoyant flame develops, creating the natural draft, pulling the combustion gases over 19 heat extraction water tubes, the exterior of the air inlet tubes, and out the stack. Several potential issues in the design will prove problematic when seeking PM emission reductions:

- The placement of firebox air at only one end of the wood load may cause uneven distribution of oxygen to the fuel bed, promoting large stoichiometry gradients in the gas phase.
- Allowing large fuel loads, the primary combustion region within the firebox is voluminous. The recombination of gas phase pyrolysis species in the pre-combustion zone is favored in large volumes, especially in fuel rich conditions<sup>3</sup>.
- The post-flame exhaust path may be too short, not allowing sufficient time for complete mixing and burnout before the gases encounter the water tubes, at which point the heat extraction effectively freezes post-flame CO and PM oxidation<sup>10</sup>. This suggests the need for a distinct and separate secondary combustion region.

## Modeling Methods

Preliminary test data are used to benchmark a CFD simulation, using FLUENT version 6.3 with a grid consisting of 104,000 tetrahedral cells. Grid dependency of solutions is avoided via adaptive refinement post-convergence. The Favre-averaged Navier-Stokes equations are solved along with enthalpy and species transport equations using finite volume discretization and SIMPLE pressure-velocity coupling<sup>11</sup>. In addition, the turbulent viscosity hypothesis is assumed valid and fluctuations are modeled by the k- $\epsilon$  model with buoyancy production. Also, radiation exchange is modeled with the Discrete Transfer Radiation Model (DTRM). To account for specific absorption bands of species mixtures, the absorption coefficient is determined by the domain based weighted-sum-of-gray-gases model (WSGGM)<sup>11</sup>. Lastly, while the physics of turbulent non-premixed flames is inherently a three-dimensional phenomenon, the loss of detail in two-dimensional modeling is assessed.

Table 1: Benchmark Modeling Summary

Run	Simulation	Fuel	Turbulent Combustion Model
1	2D Steady	CH <sub>2</sub> O	Mixture Fraction/PDF
2	3D Steady	CH <sub>2</sub> O	Mixture Fraction/PDF
3	3D Steady	CH <sub>2</sub> O	Mixture Fraction/PDF-pyrolysis limited
4	3D Steady	Mixture	Mixture Fraction/PDF
5	3D Unsteady	Mixture	Eddy-Dissipation

Wood is a highly heterogeneous fuel, comprised of various proportions of cellulose, hemicelluloses, lignin, and extractive compounds within the same tree, and this

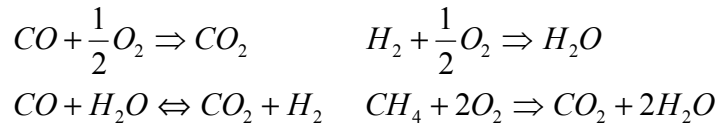
complexity is reflected in the variation of wood volatile gas constituents in the literature. To determine the best method of characterizing the gas phase oxidation, the several computational methods outlined in Table 1 were used to approach the problem.

Assuming infinitely fast and irreversible reactions, the mixture fraction approach, developed by Burke and Schumann<sup>12</sup> and Bilger<sup>13</sup>, establishes a conserved scalar Z for which the local density, temperature, and species concentrations depend upon. A preprocessor within the CFD software suite using the defined fuel and oxidizer compositions, tabulates these parameters as functions of the mean and variance of Z for several scaled heat flux scenarios in conjunction with an equilibrium chemistry solver, creating a so called “look-up table”. The effect turbulent fluctuations on the scalar field are modeled with an assumed  $\beta$ -distribution probability density function (PDF), solving the transport of its local mean and variance. The fuel pyrolysis gas is modeled as both a single surrogate species CH<sub>2</sub>O with an empirical higher heating value of 1.2278 MJ/kg<sup>14</sup> and as a mixture of CH<sub>4</sub>, CO, CO<sub>2</sub>, H<sub>2</sub>, and H<sub>2</sub>O of mass fractions 0.166, 0.465, 0.320, 0.029, and 0.019 respectively<sup>6</sup>. To prevent overestimation of fuel-rich parcel combustion, a Rich-Flammability Limit (RFL) ceases chemistry at 125% the stoichiometric mixture fraction.

$$\dot{m} = A_p S_A \rho e^{\left(-E_a/RT\right)} \quad \text{Equation 1}$$

For modeling scenario 3, the singular surrogate species mass flux boundary condition is modeled with a pyrolysis mechanism according to equation 1, based upon a zeroth order Arrhenius rate with pre-exponential constant of 4.37E+06 m/s, an activation energy of 143 kJ/mole<sup>5</sup>, local gas density, and the surface area of the cell face. This is programmed into the CFD package using a User-Defined Function (UDF).

Figure 2: Four Step Global Mechanism



Alternatively, non-equilibrium chemistry is modeled with the four-step global mechanism<sup>5</sup> shown in figure 2 using the same mixture of five species. The eddy dissipation model of Magnussen and Hjertager<sup>15</sup> is used for turbulent-chemistry interaction, based upon the assumption that the “rate of combustion will be determined by the rate of intermixing on a molecular scale of fuel and oxygen eddies”. Modeling both chemistry-limited and mixing-limited reaction rates, a finite-rate/eddy-dissipation model is used where net reaction rate of species *i* is determined by the minimum of the Arrhenius and the eddy-dissipation rates. As opposed to previous steady state simulations, this solution will be time-dependent to capture the effect of eddy dissipation on the large scale structures near the flame boundary. Convergence is determined by the asymptotic behavior of the mass-averaged stack exit temperature and CO<sub>2</sub> mass fraction, with time steps of 0.1 s.

## Boundary Conditions

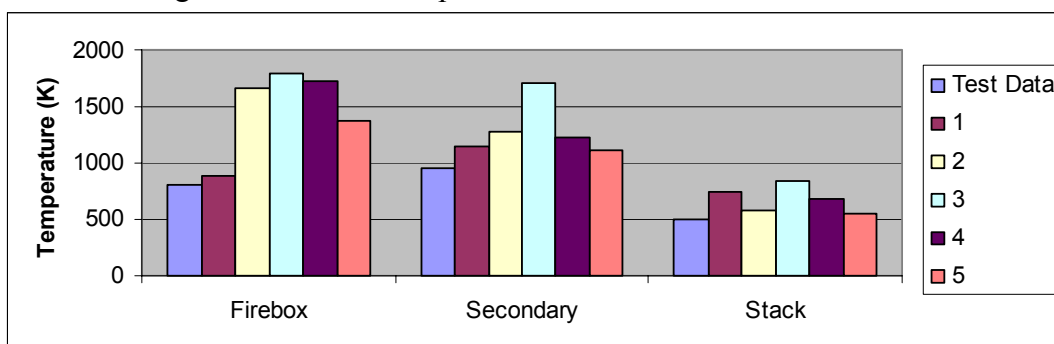
As the goal is to simulate an instantaneous snapshot of the furnace internally during the peak of gas phase pyrolysis, including the unsteady solver, the quantities from test data to be used are averaged between the 5<sup>th</sup> and 25<sup>th</sup> minute. Opacity observations suggest that this period encompasses the majority of PM emissions and also this smooths out any measurement anomalies due to sparse data sampling from a notably transient process. It should be noted that the simulation is not intended to be inclusive, rather it is determining the effects of the geometry on the flow field and the mixing of fuel and oxygen.

The mass flux of air and fuel gas entering the system, with the exception of run 3, are determined by a combination of total furnace weight loss and stack CO<sub>2</sub> and CO concentration measurements. During preliminary simulation of run 3, a runaway steady state pyrolysis rate during occurred, due to the feedback mechanism of increased local temperatures causing higher fuel emissions, causing higher flame temperatures, and so forth. To prevent this, a ceiling at the maximum observed firebox temperature is set as the steady state mass flux for each cell with the pyrolysis boundary condition algorithm. To calculate the air entering the system, the equivalence ratio is determined by considering the wood is 15% moisture on a wet basis, assuming the White Oak is  $C_{4.12}H_{5.38}N_{0.03}O_{2.70}$ <sup>16</sup>, and limiting product species CO<sub>2</sub>, CO, H<sub>2</sub>O, O<sub>2</sub>, and N<sub>2</sub>. By this analysis, the furnace is found to be running fuel rich with a total system mass air-to-fuel ratio of 3.80, compared to 4.16 at stoichiometric conditions. To avoid underestimations of intra-cell concentration gradients at the internal fuel inlet boundaries, the fuel gas is modeled as a volumetric source term in the cells adjacent to the wood surfaces. Air enters the preheating tubes at atmospheric pressure and 300 K.

Internal surface temperatures are determined by a combination of test observations and simplified heat transfer calculations. Considering the temperature of the water in the loop, the water circulation rate, estimated exhaust gas velocities, and Nusselt number correlations for flow over tube banks and flat plates<sup>17</sup>, the average water tube exterior surface temperature is estimated as 450 K. The wood surface temperature is assumed to be 573 K, the observed solid phase pyrolysis temperature<sup>6</sup>.

## Benchmark Results

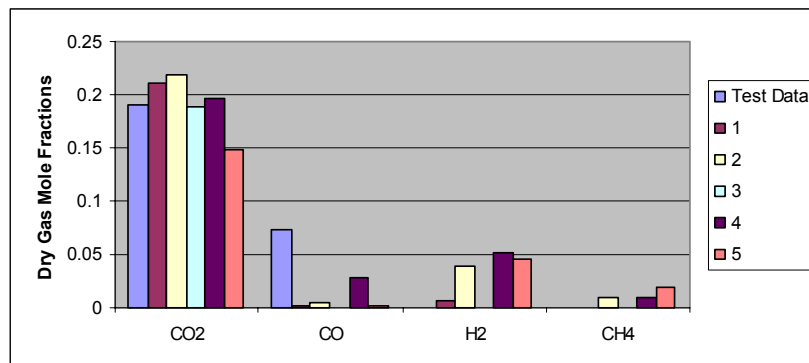
Figure 3: Internal Temperatures of Test Data vs. Simulations



The simulations are benchmarked against three temperature locations shown in Figure 1 and the measured dry gas concentrations of CO<sub>2</sub> and CO in the exhaust stream. In Figure 3, it is apparent that many methods of characterizing the gas-phase pyrolysis products and their chemistry overestimate firebox temperatures. It should be noted that the maximum flame temperature of the 2D solution is within 6.5% of the 3D mixture fraction model equivalent, run 2. The reported internal temperature at the thermocouple location is somewhat misleading, as in the 2D simulation the flame is drawn to the air side of the firebox. That said, firebox (i.e., flame) temperatures are overestimated by the mixture fraction model for the following reasons: they assume equilibrium chemistry and a limited number of product species, steady state solutions remove any influence of transient heat sinks, and local quenching of the flame by rich or humid parcels or excessive strain rates are underestimated by the assumed shape PDF with the RFL used. While better in agreement, the unsteady finite-rate chemistry run 5 also overestimated firebox temperatures by underestimating flame quenching and limiting species involved. It should be noted that the transient behavior of the measurements also may skew results, as wood log flame temperatures vary greatly within a small space<sup>6</sup>.

The secondary temperatures, located just prior to heat extraction, and the stack temperatures show better agreement with the exception of the pyrolysis limited run 3. Rather than specified by observed burn rates, the fuel pyrolysis rate is limited by the adjacent cell temperature of the wood surface and the simulated fuel burn rate is reduced from the observed 0.00663 kg(dry)/s to 0.00512 kg(dry)/s. Spatially, the pyrolysis rate is underestimated on lower logs where the colder air enters the firebox and overestimated above upper logs receiving irradiation from the flame. This causes the entire flame to lift off the logs and maximum temperatures reach beyond the secondary thermocouple location, thus overestimating combustion efficiency with a reduced fuel emission rate. Additionally, stack temperatures are overestimated due to the effectively shortened exhaust path. Run 1 stack temperatures are also underestimated due to the difficulty of representing the effect of the tube banks, and their associated heat extraction, on the flow field.

Figure 4: Stack Species Concentrations of Test Data vs. Simulations



Species concentrations of CO<sub>2</sub> and CO are mixed in their agreement with measured data. Like local density and temperature, the local concentration of a given species is solely a function of the conserved scalar Z for steady state simulations. Thus, as equilibrium

chemistry overestimates temperatures, it also overestimates the completion of combustion in the form of higher CO<sub>2</sub> and lower CO concentrations. Run 4 had a significant exhaust CO concentration due to its treatment of CO as a portion of the modeled fuel. The fuel species H<sub>2</sub> and CH<sub>4</sub> were not measured during testing, however it should be noted that they were significant portions of the simulation stack concentrations, cementing the initial determination of fuel rich operation. These species are not present in runs 1 and 3 as a result of overestimated stack temperatures.

## Benchmark Discussion

The goal of this exercise is not to identify which simulation is best suited to create a comprehensive model of the furnace from which to draw specific data points, rather it is to determine which model provides the best platform from which to explore the relative success of an operational or physical modification strategy with respect to PM formation. Additionally, it is important to select a modeling technique that requires the least amount of assumptions, while providing reasonably accurate results at a low computational cost.

Table 2: Comparative Summary of Benchmark Model Runs

Run	Pros	Cons
1	Quick convergence of 2D domain yielding reasonable agreement with data	Loss of in-plane gradients, overestimation of k and ε in 2D, and difficulty in modeling tube bank
2	Simplicity of single-species fuel yields stable solutions in less time than other 3D runs	Equilibrium chemistry approach overestimates internal temperatures and CO oxidation
3	Pyrolysis mechanism models influence of wood surface radiation over fuel emission rate providing more realistic distribution of volatilization	Requires arbitrary ceiling to prevent runaway, unstable numerical behavior requires reduced enthalpy under-relaxation factor thus slowing solution greatly, and does not allow for direct matching of observed to simulated mass burn rate
4	Mixture based fuel yields better agreeing exhaust CO concentrations	Has drawbacks of run 2 with less experimentally accepted fuel composition and less stable solution
5	Finite-rate chemistry better captures the turbulent mixing-limited reaction physics and internal temperatures compared to run 4	Unsteady solution requires a much longer simulation (+5,000 iterations)

The simulation techniques were selected for several side by side comparisons, and are summarized for their pros and cons in Table 2. Each model will be considered on a case-by-case basis when simulating the implementation of operational or physical modifications, based upon this study.

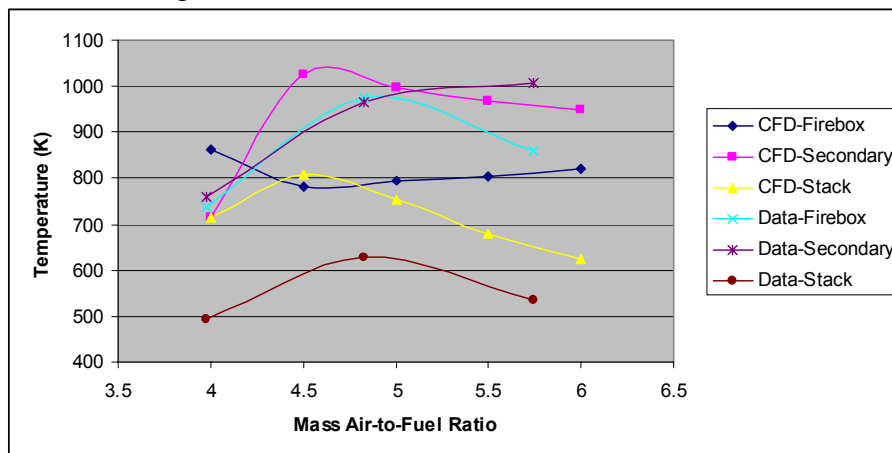
## OPERATIONAL MODIFICATIONS

The initial analysis found the Model 100 to be operating under fuel rich conditions during the first half hour of the test, at the same time the unit has significant observable PM emissions. Assuming the White Oak composition and using CO<sub>2</sub> and CO dry gas concentrations measured each minute during initial testing, the furnace has a minimum mass air-to-fuel ratio of 3.51 at the 8<sup>th</sup> minute and reaches stoichiometric air conditions at

4.16 at the 33<sup>rd</sup> minute. To determine the effect of increasing the air flow to the stoichiometric point and beyond during the peak pyrolysis period in the simulation, should indicate if the incomplete combustion that gives rise to PM emissions is strictly due to oxygen-limitations or is also mixing-limited.

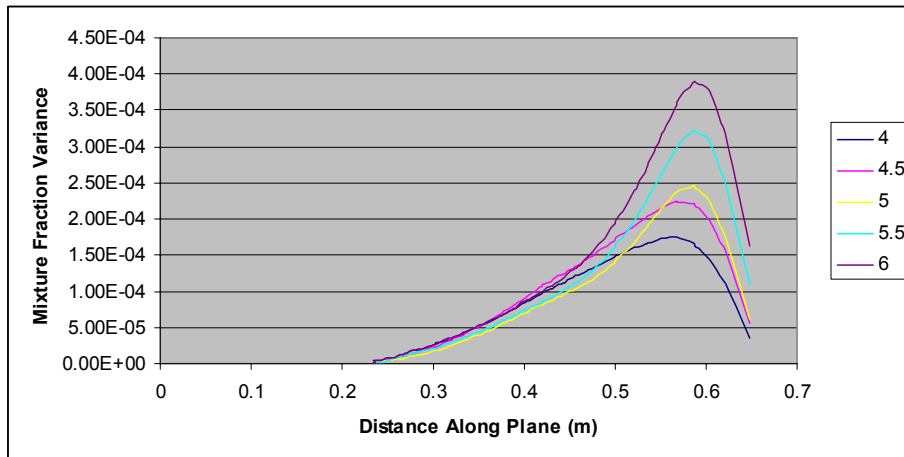
A variable speed draft induction fan is used to provide additional air during a Douglas Fir cordwood test, chemically approximated as  $C_{4.36}H_{6.3}N_{0.01}O_{2.53}$ <sup>16</sup>. With the observed burn rate, stack gas concentrations, and assumed product species, a similar analysis as done previously estimates the stoichiometric mass air-to-fuel ratio at 4.78. Simulations are performed with the modeling methods of run 1 at peak pyrolysis, with boundary conditions set by a fuel rich test data set and modified cordwood fuel geometry. The effects of additional firebox air are to be studied, starting at the observed mass air-to-fuel ratio of 3.97 and increasing up to 6.0. As chemistry is assumed to freeze upon heat extraction at the tube bank, the shortcomings of run 1 of overestimating stack temperatures and underestimating the tube bank's effect on the flow field are not important.

Figure 4: Internal Temperatures of Test Data and Simulations vs. Mass Air-to Fuel Ratio



Observed and simulated internal temperatures spike in the vicinity of the estimated stoichiometric air-to-fuel ratio of 4.78, however secondary temperatures continue to increase into lean conditions. This indicates the operation is mixing-limited as well, as the increase in secondary temperatures beyond the stoichiometric air-to-fuel ratio suggests post-flame combustion of fuel-rich parcels. The observed burn rate increased greatly indicating the prominence of the pyrolysis feedback mechanism, as moving from rich to lean conditions meant reducing test duration of similar fuel loads from 290 to 161 minutes. Achieving fuel lean conditions did reduce PM emissions, with Test Method 28 results indicating reductions from 0.3 lb PM/MMBtu input to 0.213 lb PM/MMBtu input

Figure 5: Mixture Fraction Variance Along Entrance to Tube Bank



The increase of the pyrolysis rate due to higher flame temperatures and atmospheric oxygen concentrations is not included in these simulations, however another indication of mixing-limited combustion is revealed in Figure 5. With use of the assumed shape PDF mixture fraction model, the variance of  $Z$  is a direct indicator of fuel/oxidizer mixing. A plane is created between the hot water side manifold (0.0 m) to the lip of the air side of the firebox (0.65 m) and the mixture fraction is observed for increasing air-to-fuel ratios. The peak is reached in streamlines from the flame tip and steadily increases with air added to the firebox. In addition to the increased pyrolysis rate returning the firebox creating fuel rich parcels, this may also be due to excessive strain rates quenching lower portions of the flame.

## PHYSICAL MODIFICATIONS

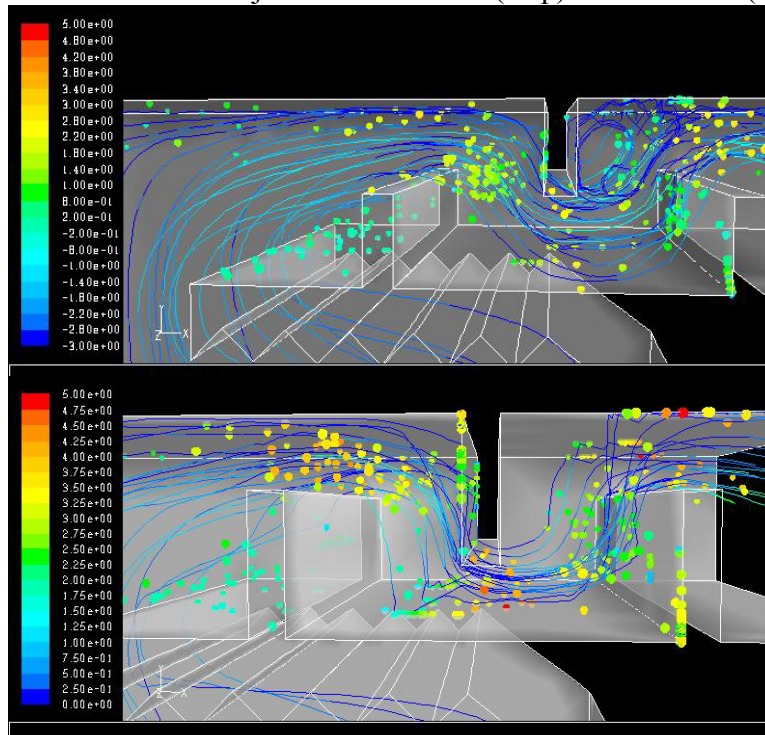
This reduction of PM emissions did come at a cost of efficiency, as evident by increased observed stack temperatures and decreased heat output rates. The feedback mechanism responsible is higher firebox temperatures due to complete combustion, which drive pyrolysis rates up and increase buoyancy (superficial velocities), which reduce the residence time of condensed PM between formation and heat extraction. The loss of efficiency and increased mixing problems can be addressed in tandem by enlarging the post-combustion zone.

One approach is to redesign the tube bank from a parallel-flow to a cross-flow mode. The cross-flow configuration significantly increases the heat transfer coefficient, allowing a more compact heat exchanger.<sup>17</sup> This modification allows additional space to be used to enhance mixing and burnout, e.g., via the addition of baffles or secondary air injection.

Flow visualization can be used to quickly evaluate baffle configuration options without the need for time-consuming experiments. We selected three baffles as a compromise between enhancing mixing and adding hardware. The goal is to determine the configuration that maximizes particle residence times, via departure from mean flow

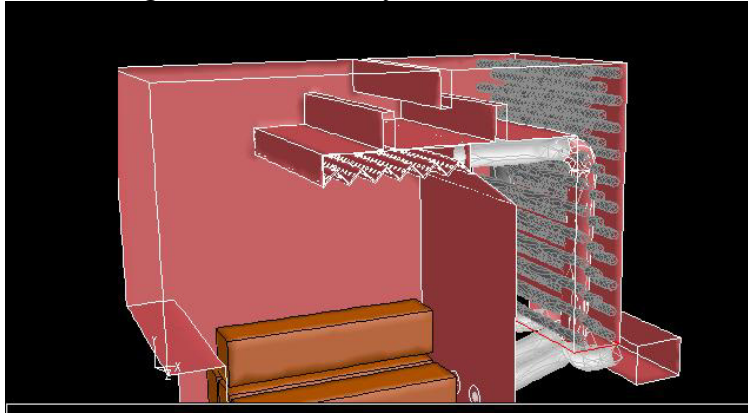
pathlines, while minimizing the total pressure drop. This redesign requires the use of a blower at the air inlets sized at 216 cfm at 0" WC static pressure.

Figure 6: Pathlines & Particle Trajectories for Flush (Top) & Non-flush (Bottom) Baffles



A non-reacting CFD simulation is performed for various configurations, with air at typical exhaust mass flow rate of 0.1 kg/s observed during experiments with the blower, laden with inert  $1 \mu\text{m}$  particles of density  $1,500 \text{ kg/m}^3$ . While there was little difference between configurations of up-down-up or vice versa, Figure 6 illustrates the difference between baffles that extend 1" into and that are flush with the vertical midpoint of the flow path. The figure shows the pathlines of the flow field as solid lines colored by velocity magnitude and the particle positions, exaggerated in size for clarity and colored by x-velocity, after 10 s of time-stepping. Note that the both graphics are scaled such that the particles are colored by the upper scale and the pathline velocity magnitudes are colored by the lower scale. Lower x-velocities of the particles and locations outside of pathlines, including wall impaction, are desired. There is little distinction between the two configurations with respect to dispersion of particles outside of the mean flow pathlines, however the non-flush baffles exhibit the tendency of pathline compression and stratification past the baffle tip. This increases particle x-velocities, thus reducing residence times, and reduces circulation zones that entrain particles as seen after the second flush baffle. Additionally, the non-flush baffles have a pressure drop of 0.096" WC greater than the flush baffles. Therefore the flush baffles were selected for implementation.

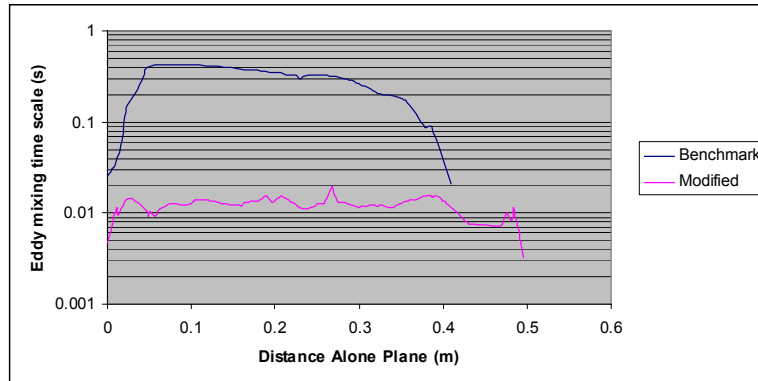
Figure 7: OWHH Physical Modifications



A full reacting CFD simulation is performed using the redesigned geometry, as seen in Figure 7, for a cribwood fuel load to directly compare to the benchmarked runs. In addition to the implementation of baffles, a hollow shelf, or “airbox”, is placed above the firebox from which secondary air is injected downwards onto the flame. As transient 3D effects on the turbulence-limited chemistry are important, the model assumptions of run 5 are used. Boundary conditions are identical to that of run 5 with the exception of the increased blower air of 120 cfm, based upon assumed internal pressure losses and fan speed.

Comparing simulation results to the benchmark run 5 show great improvement in combustion efficiency, with trace concentrations of  $H_2$  and  $CH_4$  at the firebox exit. This is a result of the secondary injection of overfire air and overall fuel lean operation. As a result, the dry mole fraction of  $O_2$  at the outlet is 0.092, which should be reduced for a marketable furnace.

Figure 8: Turbulent Mixing Along Entrance to Tube Bank



In the absence of a mixture fraction variance, the improvement in mixing rate may be assessed directly through use of the eddy dissipation model<sup>15</sup> of turbulent-finite rate chemistry interactions. The model postulates that reaction rate kinetics is inversely proportional to the eddy mixing time scale,  $k/\epsilon$ . Within the model, this time scale acts as a switch to initiate chemistry without the need for an ignition source<sup>11</sup>. Figure 8 compares this time scale along plane just prior to the tube banks for the benchmark and

modified furnace, with the depth-wise and height-wise midpoints used respectively. As a result of the physical modifications, the eddy dissipation rate is increased by an order of magnitude.

By virtue of operating fuel lean and increasing mixing during simulations, the combustion efficiency is improved, thus PM emissions reductions are expected. While PM emissions sampling has not been performed on this physically modified furnace, cordwood testing has shown peak pyrolysis stack temperatures reduced to 365 K, test duration increased to 295 minutes, and an efficiency of 46.8% based upon fuel input.

## **SUMMARY**

A commercial CFD suite was used successfully as a 2D and 3D modeling tool in reducing the PM emissions and addressing overall efficiency of a commercially available OWHH. While PM formation and oxidation is not modeled directly, due to the lack of a non-empirical comprehensive model, the combustion efficiency is used as a metric of expected PM emissions. The gas phase oxidation of the wood was modeled exclusively and the fuel gas was modeled as either an empirical surrogate  $\text{CH}_2\text{O}$  or a mixture of  $\text{CH}_4$ ,  $\text{CO}_2$ ,  $\text{CO}$ ,  $\text{H}_2$ , and  $\text{H}_2\text{O}$ . An Arrhenius type pyrolysis rate was modeled with mixed success. Turbulent chemistry interactions were modeled using the steady state assumed shape PDF mixture fraction and transient finite-rate chemistry eddy-dissipation models. The mixture fraction approach, due to an assumption of equilibrium chemistry and limited product species, consistently overestimates internal temperatures and thus completeness of combustion. Reasonable agreement is found with EPA Method 28 test data, however the relative strengths and weaknesses of each approach do not allow for a “one size fits all” selection.

Operational and physical modifications of the OWHH were simulated with the benchmarked models. Upon identifying the OWHH operation as fuel rich from analysis of the data, the effect of incrementally increased mass air-to-fuel ratio is modeled for a cordwood fuel load. Mixture fraction variance, an indication of the degree of species mixing, worsens with increasing firebox air at just prior to heat extraction, where temperatures are observed to drop and chemistry is assumed to freeze. Test results with increased firebox air indicated a PM emissions reduction by 29% but also an increase of stack temperatures by up to 134 K. To address the loss of efficiency and species mixing, a compact heat exchanger is determined analytically feasible, enlarging the post-combustion zone. Secondary over-fire air jets and baffles are to be implemented, with the aid of flow visualization with a cold-flow CFD discrete particle model selecting the optimum baffle configuration. A full reacting CFD simulation indicates lean operation and an order-of-magnitude increase in mixing prior to heat extraction. Cordwood testing results show an efficiency of 46.8% based upon fuel input.

## **Acknowledgements**

This work was supported through a Research & Technology Development grant, administered by the Washington Technology Center and funded in part by Greenwood

Technologies and the University of Washington. Thanks are owed to technical support from Dr. Renata Bura, Dr. James Riley, K. Boyd Fackler, and the staff of Greenwood Technologies.

## REFERENCES

1. U.S. Department of Energy, Energy Information Administration, *A Look at Residential Energy Consumption in 2001*
2. Tillman, D.A.; Rossi, A.J., Kitto, W.D.; *Wood Combustion: Principles, Processes, and Economics*; Academic Press: New York, NY, 1981.
3. Fine, P.M.; Cass, G.R., Simonett, B.R.T.; *Environmental Science Technology*, **2001**, *35*, 2665-2675.
4. Fitzpatrick, E.M.; Ross, A.B., Bates, J.; Andrews, G.; Jones, J.M.; Phylaktou, H.; Pourkashanian, M.; Williams, A.; *Process Safety and Environmental Protection, Institution of Chemical Engineers*, **2007**, *85 (B5)*, 430-440.
5. Galgano, A; Di Blasi, C.; *Progress in Computation Fluid Dynamics*, **2006**, *6*, Nos. 4/5, 287-302.
6. Huttenen, M.; Saastamoinen, J.; Kilpinen, P.; Kjaldman, L.; Oravainen, H.; Boström, S.; *Progress in Computation Fluid Dynamics*, **2006**, *6*, Nos. 4/5, 200-208.
7. Bai, X.S., Griselin, N.; Klason, T.; Nilsson, J.; *CFD Modeling of Biomass Combustion in Small-Scale Boilers - Final Report*; Division of Fluid Mechanics, Department of Heat and Power Engineering, Lund Institute of Technology, Lund, Sweden, 2002.
8. *Test Method 28: Certification and Auditing of Wood Heaters*; U.S. Environmental Protection Agency.
9. Kronenburg, A.; Bilger, R.W.; Kent, J.H.; *Combustion and Flame*, **2000**, *121*, 24-40.
10. Turns, S.R.; *An Introduction to Combustion*, 2<sup>nd</sup> Ed.; McGraw Hill: Boston, MA, 2000.
11. *FLUENT 6.3 User's Guide*, 2006
12. Burke, S.P.; Schumann, E.W.; *Combustion Symposium, Industrial and Engineering Chemistry*, **1928**, *20*, 998-1004.
13. Bilger, R.W.; *Combustion Science and Technology*, **1976**, *13*, 155-170.

14. Bhaskar Dixit, C.S.; Paul, P.J.; Mukunda, H.S.; *Biomass and Bioenergy*, **2006**, *30*, 684-691.
15. Magnussen, B.F.; Hjertager, B.H.; *16<sup>th</sup> International Symposium on Combustion, The Combustion Institute*, **1976**.
16. Bain, R.L.; Amos, W.A.; Downing, M.; Perlack, R.L.; U.S. Department of Energy, National Renewable Energy Laboratory, *Biopower Technical Assessment: State of the Industry and Technology*, 2003.
17. Incropera, F.P., DeWitt, D.P.; *Introduction to Heat Transfer*, 4<sup>th</sup> Ed.; John Wiley & Sons: New York, NY, 2002.